
Article:
Dawson, J.A., Sinclair, D.C., Harding, J.H. et al. (1 more author) (2014) A-Site Strain and Displacement in Ba1-xCaxTiO3 and Ba1-xSrxTiO3 and the Consequences for the Curie Temperature. Chemistry of Materials, 26 (21). pp. 6104-6112. ISSN 0897-4756

https://doi.org/10.1021/cm502158n

A-site Strain and Displacement in $Ba_{1-x}Ca_xTiO_3$ and $Ba_{1-x}Sr_xTiO_3$ and the Consequences for the Curie Temperature

James A. Dawson,[†] Derek C. Sinclair,[‡] John H. Harding,[‡] and Colin L. Freeman[*,‡]

Department of Materials Science and Engineering, Kyoto University, Sakyo-ku, Kyoto, Japan, and Department of Materials Science and Engineering, University of Sheffield, Sheffield, UK

E-mail: c.l.freeman@sheffield.ac.uk
Phone: +44 (0)114 222 5965. Fax: +44 (0)114 222 5943

Abstract

Classical computer simulations are performed on the whole solids solution range of $Ba_{1-x}Ca_xTiO_3$ (BCT) and $Ba_{1-x}Sr_xTiO_3$ (BST). The enthalpies and volumes of mixing are produced and a full local structural analysis is performed. The simulations demonstrate that large degrees of disorder form in the BCT solid solution which leads to distortions in the TiO_6 octahedra. Comparing the positions of Sr in BST and Ca in BCT, the position of the Sr cation is largely central within the dodecahedra while the position of the Ca is significantly off-centre in many configurations. The relaxation is associated with a shift towards an eight coordinate site compared to a twelve coordinate cation. An empirical model is fitted for predicting the Curie Temperature of the solid solution based on the local structure which shows excellent agreement with experimental values.

Introduction

The ability of the ABO_3 perovskite structure of compounds such as $BaTiO_3$ and $CaTiO_3$ to accept isovalent dopants on both the A- and B-sites is crucial in manipulating their electrical properties. While B-site doping of $BaTiO_3$ can have a dramatic effect on both the permittivity and the phase transition temperatures of the compound,[1–3] A-site doping is often used to alter the ferroelectric Curie temperature (T_c) in addition to other phase transition temperatures such as the tetragonal to orthorhombic transition.[4–6] Common A-site isovalent dopants for these materials are other alkaline earth metals such as Ca^{2+}, Ba^{2+} and Sr^{2+} or similarly sized post-transition metals e.g. Pb^{2+}.

As a result of the importance of the electrical properties of these materials (which include ferroelectricity and high intrinsic permittivity[7–10]), there has been a significant amount of work on both the undoped compounds and mixed compounds over the full solid solution range. For the $Ba_{1-x}Sr_xTiO_3$ mix (BST) complete solubility exists and T_c decreases with increasing Sr^{2+} concentration as the smaller ion stabilises the cubic phase.[11]

The solid solution limit for the $Ba_{1-x}Ca_xTiO_3$ system (BCT) is only 24 mol% due to the increased size mismatch between the two A-site cations[6] beyond which there exists a phase mixture of tetragonal BCT and orthorhombic $Ca_{1-x}Ba_xTiO_3$ (CBT). Furthermore, an unusual

*To whom correspondence should be addressed
[†]Department of Materials Science and Engineering, Kyoto University, Sakyo-ku, Kyoto, Japan
[‡]Department of Materials Science and Engineering, University of Sheffield, Sheffield, UK

T_c effect is also observed for this mixed compound; T_c rises from 403K for undoped $BaTiO_3$ to 410K for 8 mol% Ca concentration and then decreases up to the solid solution limit.[6,11] This anomaly cannot be explained by a simple cation size effect as for the Sr-doped compound. Sinclair and Attfield[11] suggest the initial increase in T_c should be attributed to a strain effect associated with size mismatch of Ca and Ba on the A-site, whereas the decrease in the T_c for compositions with $x > 8$ mol% Ca should be attributed to a size effect. Reverse monte carlo refinements of a range of experimental data show the existence of ferroelectric Ca displacements caused by strain in Ca-O bonds.[12] It is suggested that the sustained T_c is a direct result of the Ca displacements and this effect is in competition with the reducing average octahedral volume. Ca K-edge extended X-ray absorption fine structure (EXAFS) has also been used to confirm that the average Ca-O interatomic distance in BCT is longer than in $CaTiO_3$.[13] The potential for A-site displacements to contribute to the ferroelectric properties of BCT has been previously shown by X-ray absorption near edge structure XANES spectroscopy[14] and *ab initio* calculations.[14,15] Okajima *et al.*[14] used Ca K-edge XANES and DFT calculations to show that Ca ions substitute at Ba sites and this substitution caused a small displacement in the c-axis. It has also been suggested that the polarisation arising from Ca displacements works cooperatively with Ti-O distortions and that this stabilises the tetragonal phase of BCT.[15] No similar off-centring has been observed for BST.

A fundamental problem with these systems as highlighted by experimental studies e.g.[12] is the large degree of disorder within the materials that makes analysis of average experimental signals extremely difficult. It also means that *ab initio* studies may struggle as these can model only very small cells and not tackle a wide range of varying relaxations that may take place in a disordered material.

Here, we use classical simulation methods, specifically lattice statics, with a new forcefield to explore the enthalpy of mixing of BST and BCT solid solutions. Because of the relatively small expense of classical simulations we are able to optimise thousands of large cells and analyse the configurations and structures in detail. By doing this we can create an ensemble of the solid solution accounting for the large degree of variation and disorder present. Using this method we assess how viable different explanations currently within the literature are to explain the unusual T_c behaviour in BCT.

Computational Methods

The General Utility Lattice Program (GULP)[16] was used to perform all the calculations presented here. The forcefield for the ceramics is described with a Born model where the atoms are treated as charged spheres (with their formal atomic charges) with attractive and repulsive short range interactions being simulated by the interatomic potentials. In the static limit, lattice vibrations are ignored and the structure is determined by the static contribution to the internal energy, therefore exact agreement with experiments carried out at various temperatures and pressures cannot be expected. Ionic polarisation is taken into account by the shell model developed by Dick and Overhauser.[17] Detailed reviews of these well established techniques are available elsewhere.[18]

The potential set combines a $BaTiO_3$ potential set developed for the study of Rare-Earth (RE) doping[19] with recently published Sr-O and Ca-O interatomic potentials[20] and a cutoff of 12 Å for all potentials. A three body O-Ti-O term is also used to represent the covalent character of the Ti-O bond. A detailed description of the fitting procedure for this $BaTiO_3$ potential set is available in.[19] The Sr-O and Ca-O interatomic potentials were fitted to both the lattice energies and lattice parameters of their respective oxide and titanate.[20]

In the solid solution a potentially huge variety of different configurations will be present due to the large number of different arrangements available to cations on the A-site. Of these k configurations, only the low energy ones will contribute significantly to the overall thermodynamic properties of the solid solution. Therefore to sample the system effectively we must generate the energies for a large number of different low energy configurations, then generate the partition function for the ensemble and then the enthalpy, H, i.e.

$$H = \frac{\sum_{k}^{K} H_k \exp(-H_k/k_B T)}{\sum_{k}^{K} \exp(-H_k/k_B T)}, \qquad (1)$$

where H_k is the energy of configuration k, k_B is the Boltzmann constant, and T is the temperature. To generate these configurations we use a genetic algorithm (GA) method previously described.[21] With this method we begin from ten different random configurations at a given solid solution mix and perform full geometry optimisations on each configuration. Ten new configurations are then generated by mixing pairs of these configurations together. The selection of the configurations used for the mixing (breeding) is governed by the relaxed energy of each configuration - the lower this value the more likely they are to be used. This ensures the system preferentially selects configurations that are lower in energy and therefore more important towards the overall thermodynamic properties of the ensemble. This breeding process then continues for twenty cycles. This operation gradually optimises the energy of the configurations to lower energies while still sampling a large number of different configurations. After each breeding cycle each configuration has a random chance of being mutated (10%) where two atoms are randomly swapped in the configuration (e.g. a Ca and Ba are swapped over). This high mutation rate ensures that new configurations are introduced into the process preventing trapping in localised energy wells. A minimum of eight GA runs were attempted for each solid solution mix generating approximately 2,500 unique configurations for each mix. In all mixes, by the end of the 20 breeding cycles, the same lowest energy configuration was found for each of the 8 runs which suggests the GA is falling into a significant and potentially the lowest energy minimum in the solid solution. A 4x4x4 cell was used for all the simulations containing a total of 64 formula units and the solid solutions of $Ba_{1-x}A_xTiO_3$ were studied for the whole solid solution range in BCT and BST. This cell is large enough to generate both isolated and aggregated defects within the system to study the importance of organisation of the cations within the solid solution.

Ideally, a tetragonal $BaTiO_3$ structure would have been used for simulating the BST and BCT solid solutions to correspond with experiment.[11] Unfortunately due to the small difference between lattice parameters (c/a = 1.0128) energy minimisations will favour the higher symmetry cubic structure and therefore the cubic $BaTiO_3$ structure has been used in these calculations. These phases are structurally similar and the local relaxations caused by defects are also likely to be similar or even the same. As the focus of this work is to investigate the structural and energetic effects, it is therefore reasonable to suggest this will not influence the conclusions.

In addition to the thermodynamic mixes, larger cells were optimised to check for possible effects of localised ordering and to examine low concentrations. Cells of 7x7x7 formula units were optimised for mole fraction values of Ca,Sr of x = 0.0058, 0.0350, 0.0787, 0.1166, 0.1458, 0.1983 and 0.2391.

Results and discussion

Thermodynamics of Mixing

The enthalpy of mixing, ΔH_{mix}, curves for BST and BCT are shown in Figure 1. The ΔH_{mix} is positive for all values (with the exception of x=0.9375 for BST). The ΔH_{mix} values for BST are far smaller than those of BCT and at 50% a total ΔH_{mix} (Sr-Ba) of 0.0057 eV is obtained, which is well below RT (0.02 eV at 298 K). This corresponds well with experimental findings that complete solubility occurs in this system.[11,22] Such low energies also suggest the Ti-O interaction is by far the most dominant interaction in the system as the formation of the solid solution has only a small effect on the energetics in comparison with the pure end members. The curve is close to symmetric which suggests that doping Sr into BT is as easy as doping Ba into ST. The values for BCT are far larger and are larger than RT at x$\geq$0.0625. Experimentally the solid solution limit has been reported at x=0.24[23] at which our simulations report a ΔH_{mix} of $\sim$5RT. The large size mismatch between the Ca (1.00 Å) and Ba (1.38 Å) cations means the two ions cannot readily coexist in the

lattice without causing large levels of strain. In $CaTiO_3$ the Ca cation has an eight-fold coordination compared to the 12-fold coordination in BT and therefore the ions do not readily occupy each other's site.

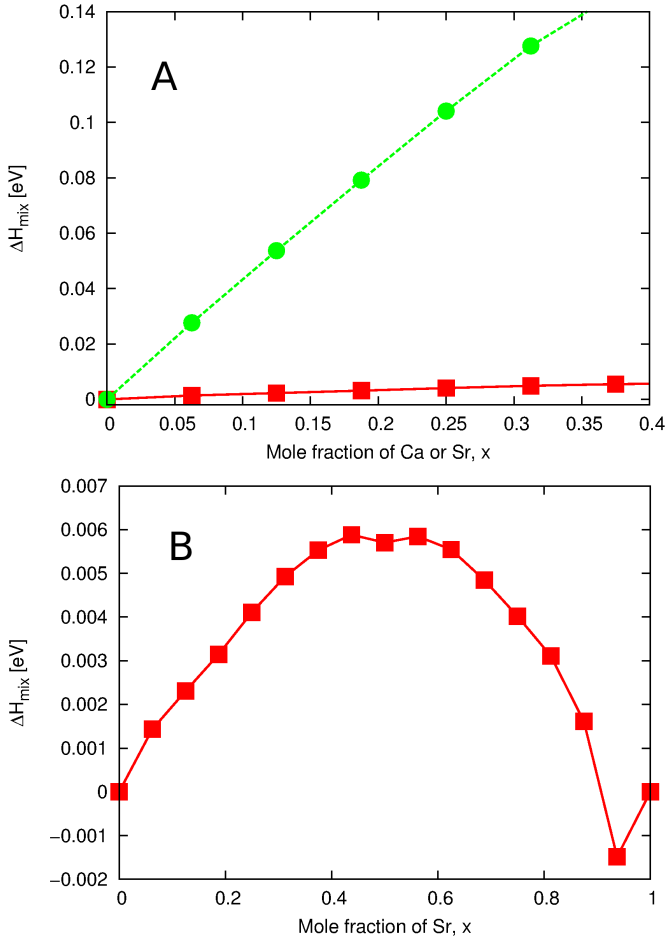

Figure 1: Calculated enthalpy of mixing curves for $Ba_{1-x}Ca_xTiO_3$ (green circles) and $Ba_{1-x}Sr_xTiO_3$ (red squares). (A) shows both mixing systems up to x=0.4 (B) shows the whole mixing range for $Ba_{1-x}Sr_xTiO_3$.

The volumes of mixing, ΔV_{mix}, curves are plotted in Figure 2 for BST and BCT. These support the findings of the enthalpy curves. The BST mixing curve shows a generally negative deviation from an ideal mix and at low Sr and Ba content there are large deviations from ideality with significant shrinkage of the cell. For BCT a large positive deviation from ideal mixing is observed in agreement with experiment. This is due to the differences in the preferred coordination of the cations (8 for Ca vs 12 for Ba) which will cause large degrees of strain and distort the surrounding lattice leading to increases in the volume compared to that expected from ideal mixing. We will discuss the unusual behaviour of the mixing and enthalpy at very low Sr or Ba concentrations later.

Table 1: Volume of unit cell (Å^3) for $Ba_{1-x}Ca_xTiO_3$ and $Ba_{1-x}Sr_xTiO_3$.

Mole fraction	$Ca_xBa_{1-x}TiO_6$	$Sr_xBa_{1-x}TiO_6$
0.0625	64.01	64.16
0.125	63.80	63.99
0.1875	63.56	63.89
0.25	63.30	63.75
0.3125	63.00	63.63
0.375	62.64	63.50
0.4375	62.34	63.37

The volume of the cell shrinks with increasing Sr and Ca content (Table 1). This agrees well with experiment for BST[24] and more recent analysis of BCT.[12] Adding a smaller cation should cause a shrinkage of the cell as the Sr-O/Ca-O separations will be shorter than the Ba-O separations.

Partitioning and Organisation

No ordering or defect segregation is observed amongst the wide range of configurations calculated. In general there is a very small spread of energies across nearly all the configurations calculated, which suggests homogeneous mixing throughout the solid solution. This implies that the local environment (i.e. the nearest neighbours) is the crucial component in determining the energy of a configuration and no significant medium-long range ordering occurs in the lattice.

Local Structural Analysis

TiO_6 Octahedra

We now analyse the local relaxations that occur throughout the solid solution and compare to the other experimental and theoretical studies. We have highlighted the TiO_6 octahedra as crucial for determining much of the energetics and properties (specifically the ferroelectric behaviour) of the system and therefore it is instructive to examine their structure in the solid solution. We observe a general trend of decreasing octahedral volume

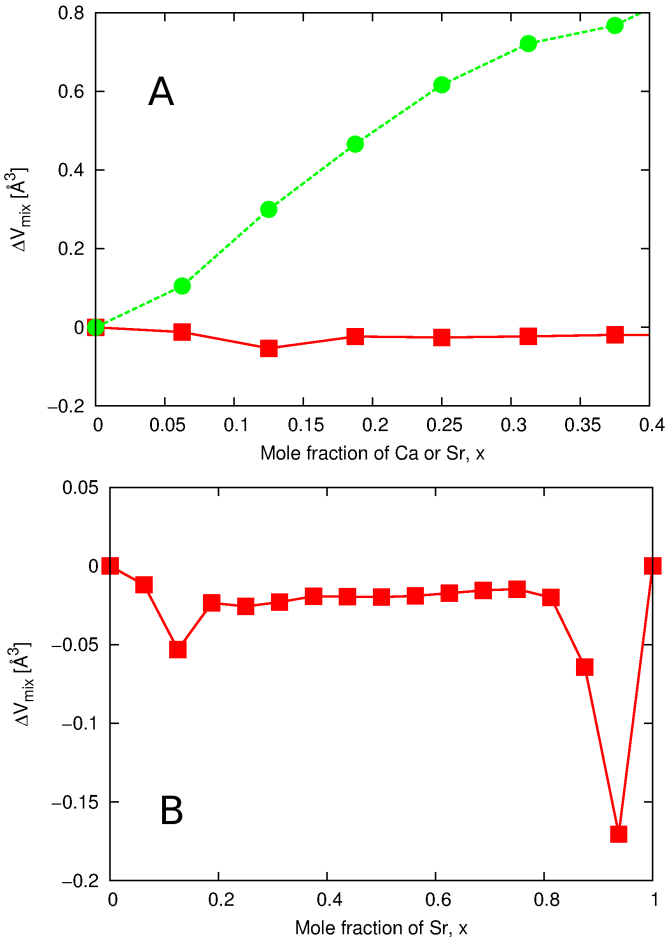

Figure 2: Calculated volume of mixing curves for $Ba_{1-x}Ca_xTiO_3$ (green circles) and $Ba_{1-x}Sr_xTiO_3$ (red squares). (A) shows both mixing systems up to x=0.4 (B) shows the whole mixing range for $Ba_{1-x}Sr_xTiO_3$.

with increasing mole fraction of both Sr and Ca as shown in Figure 3. Overall the cell is shrinking and therefore we would also expect to see a shrinking of the octahedra. As would also be expected the octahedra shrink faster with the smaller Ca cation compared to the larger Sr cation. The maximum and minimum values reported for the octahedral volume indicate that some disorder exists within the solid solution and the octahedra do not relax uniformly. Even with a value of x=0.0058 there is a variation of $>$0.1 Å^3 and this increases with increasing Sr or Ca content. Up to the solid solution limit in BCT, the largest octahedra still have a volume equivalent to undoped BT (10.718 Å^3) which indicates that many of the octahedra are not significantly shrinking or relaxing at all. Beyond the solid solution limit in BCT

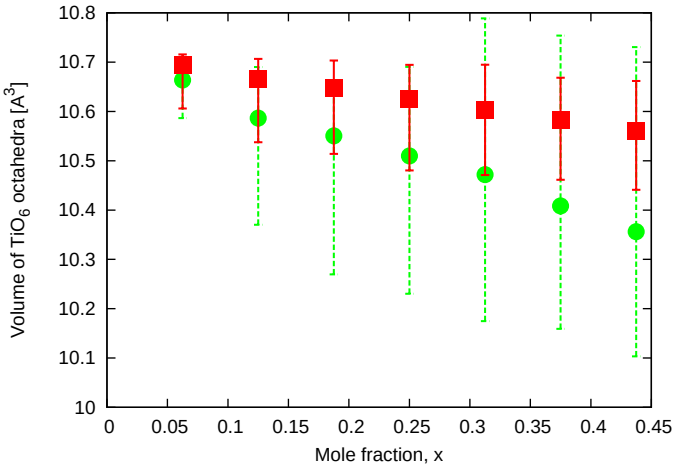

Figure 3: Average volume of all the TiO_6 octahedra at each mole fraction (x) in $Ba_{1-x}Ca_xTiO_3$ (green circles) and $Ba_{1-x}Sr_xTiO_3$ (red squares). The error bars indicate the maximum and minimum volume recorded across all the samples.

a large variation in the octahedral volume is observed which is indicative of large scale structural distortions which are energetically expensive and suggests why the experimental solid solution limit exists. The variation of the volume in BST is smaller than BCT but is still significant.

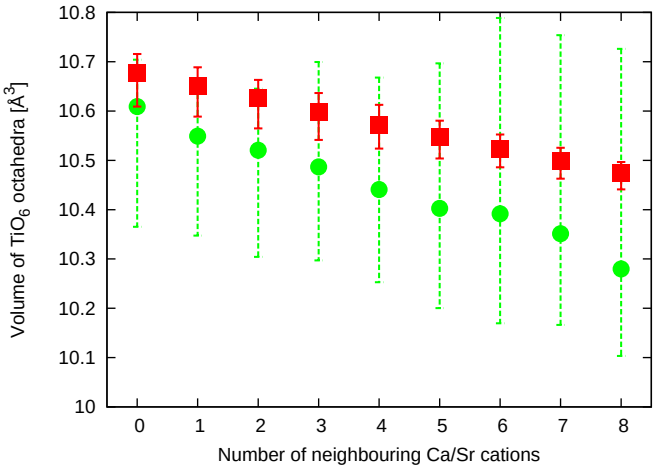

Figure 4: Average volume of all the TiO_6 octahedra with the number of neighbouring Ca,Sr cations to the Ti in $Ba_{1-x}Ca_xTiO_3$ (green circles) and $Ba_{1-x}Sr_xTiO_3$ (red squares). The error bars indicate the maximum and minimum volume recorded across all the samples.

A similar analysis can be performed by looking at the volume variation with the number of Ca or Sr neighbours to the octahedra (Figure 4) which

shows for BST that the more Sr there are neighbouring the Ti the smaller the octahedra although we do not observe as large a reduction as Levin *et al*[12,24] where values down to ∼9.7 Å^3 with 5 Sr neighbours were reported. As Sr surround the octahedra two effects are observed. Firstly, in low concentrations the Sr will potentially struggle to fill the larger Ba site and therefore some of the Oxygen anions will be pulled in closer to the Ti reducing the volume of the octahedra and also explaining the large negative ΔV_{mix} observed at low Sr concentrations in the solid solution (Figure 2). Secondly, as the number of Sr increases around the octahedra the entire region of the cell will shrink as the Sr-O separations are shorter than Ba-O which will pull the Oxygen anions within the faces of the octahedra closer together and shrink the volume.

The average octahedral volume also reduces with increasing numbers of neighbouring Ca cations in contradiction to the reverse monte carlo fitting of Levin *et al.*[12] The octahedral volume does have a very large variation with the maximum volumes largely independent of the number of neighbouring Ca as also seen for the total Ca mol fraction. The increasing octahedral volume reported in[12] would rely on all the Oxygen anions being pulled away from the central Ti towards the Ca that neighbour each face. This basic process would suggest a very large scale distortion and possibly destruction of the octahedral shape when multiple Ca are present and is at odds with the suggested model of Ca relaxation along the [111] direction towards the faces of the octahedra. The large variation of the volumes again indicates no simple single relaxation takes place and we must view the solid solution as a more complex system with lots of internal local relaxations and fitting a single universal relaxation is not possible. This would have made successful fitting with the reverse monte carlo extremely challenging.

We have examined the level of disorder within the octahedra by comparison of the volume of the four separate TiO_3 tetrahedra that make up each octahedron and calculating the standard deviation of their volume distribution (Table 2). As expected for BST the four tetrahedra all generally have a similar volume and the octahedra are relatively regular. In the case of BCT we see standard deviation values at least twice as large as for BST.

Table 2: Average TiO_6 volume in $Ca,Sr_xBa_{1-x}TiO_6$ for a mix of mole fraction (x). The standard deviation of the volumes of the four tetrahedra that constitute a single octahedron are also listed.

	Average octahedron volume Å^3	
Mole fraction	$Ca_xBa_{1-x}TiO_6$	$Sr_xBa_{1-x}TiO_6$
0.0625	10.664 ± 0.018	10.693 ± 0.010
0.125	10.586 ± 0.042	10.665 ± 0.017
0.1875	10.551 ± 0.053	10.645 ± 0.021
0.25	10.510 ± 0.057	10.625 ± 0.024
0.3125	10.472 ± 0.060	10.604 ± 0.027
0.375	10.408 ± 0.060	10.582 ± 0.028
0.4375	10.356 ± 0.062	10.560 ± 0.029

This implies the octahedra are being distorted in BCT with some tetrahedra compressing significantly compared to others.

Cation-Oxygen Separations

Calculations on 7 x 7 x 7 (1715 atoms) supercells were used to investigate the effect of increasing Ca or Sr mole fraction on Ba-O, Ca-O and Ti-O interatomic distances. The average cation-Oxygen separations are listed in Table 3 along with the maximum and minimum separations at each mole fraction. The Ti-O separations gradually decrease as the amount of Sr/Ca is increased in line with the reduction in the volume of the octahedra with smaller Ti-O separations in BCT/BST. The average value however, varies by less than 0.01 Å demonstrating the stiffness of this bond. The range of Ti-O separations is important as the ability for disorder within the octahedra is crucial to the tetragonal relaxation. The range between maximum and minimum Ti-O separation in BCT is approximately double that of BST again demonstrating greater disorder in the BCT system.

In BST the average Ba,Sr-O separation varies by only 0.001 Å over the composition range and the difference between the Sr-O and Ba-O separations is only ∼0.03 Å. The maximum and minimum values of the Sr-O and Ba-O also vary over the range by a maximum difference of 0.09 Å and 0.08 Å, respectively which suggests the AO_{12} dodecahedra are remaining relatively regular and the A-site cation remains reasonably central within them.

Table 3: Average A or B-O separations (where A=Ca,Sr and B=Ti) in Å for $(Ca,Sr)_xBa_{1-x}TiO_6$ for a mix of mole fraction (x).

$Ba_{1-x}Sr_xTiO_3$	Separation (min - mean - max)		
Mole fraction	Sr-O	Ba-O	Ti-O
0.0058	2.806 - 2.807 - 2.808	2.825 - 2.833 - 2.862	1.998 - 2.003 - 2.006
0.035	2.785 - 2.807 - 2.851	2.813 - 2.833 - 2.869	1.989 - 2.002 -2.009
0.079	2.777 - 2.807 - 2.851	2.806 - 2.832 - 2.873	1.985 - 2.001 - 2.009
0.117	2.774 - 2.806 - 2.853	2.803 -2.832 - 2.875	1.983 - 2.000 - 2.010
0.146	2.770 - 2.806 -2.855	2.803 - 2.832 - 2.872	1.982 - 2.000 - 2.009
0.20	2.766 - 2.806 - 2.856	2.801 - 2.832 - 2.878	1.983 - 1.999 - 2.009
0.239	2.766 - 2.806 - 2.858	2.794 - 2.832 - 2.875	1.981 - 1.998 - 2.009

$Ba_{1-x}Ca_xTiO_3$	Separation (min - mean - max)		
Mole fraction	Ca-O	Ba-O	Ti-O
0.0058	2.782 - 2.785 - 2.787	2.818 - 2.833 - 2.889	1.994 - 2.003 - 2.008
0.035	2.701 - 2.785 - 2.921	2.793 - 2.833 - 2.901	1.979 - 2.002 -2.014
0.079	2.691 - 2.784 - 2.915	2.783 - 2.832 - 2.920	1.972 - 2.000 - 2.014
0.117	2.680 - 2.783 - 2.932	2.775 -2.832 - 2.915	1.970 - 1.998 - 2.015
0.146	2.670 - 2.783 -2.960	2.774 - 2.831 - 2.919	1.965 - 1.997 - 2.014
0.20	2.587 - 2.782 - 3.073	2.736 - 2.831 - 2.946	1.967 - 1.995 - 2.015
0.239	2.541 - 2.782 - 3.072	2.746 - 2.831 - 2.978	1.963 - 1.994 - 2.015

Comparing this to BCT, a slightly larger variation in the mean A-O separation over the composition range and a larger difference between the average Ca-O and Ba-O separations is observed as expected since the ionic radius of Ca is smaller than Sr. What is much more striking is the very large variation between the maximum and minimum A-O separations. These are as large as 0.53 Å and 0.23 Å for Ca-O and Ba-O, respectively (x=0.24). The largest Ca-O separation actually becomes greater than the largest Ba-O separation at x>0.12 in agreement with refs.[14,25] This implies many of the dodecahedra are becoming highly irregular and/or the A-site cation is moving far from the central position.

The relaxations identified previously suggest Ca is reducing its coordination. Ca would normally be found with lower coordination values than the 12 in BCT, e.g. 6 in lime (CaO) and calcite ($CaCO_3$), 8 in $CaTiO_3$ and 9 in aragonite (a high pressure form of $CaCO_3$), which suggests the site in BT is too large for this cation. The Ca-O distances calculated for orthorhombic-$CaTiO_3$ range from 2.34 to 2.66 Å. It is not surprising, therefore, that Ca is too small for the A-site and it will undergo a relaxation to reduce its coordination. Figure 5 shows the distribution of the Ca-O and Ba-O separations of the BCT system for x=0.08 (the other mole fractions are plotted in the supplementary information and show a similar distribution). Three peaks are observed in the Ca-O separations from a mole fraction of x=0.04-0.2 which implies two different Ca-O coordination values are present in the system: one where all 12 of the Ca-O separations remain relatively similar and the Ca remains central within the dodecahedra (the middle peak only) and the second where three different Ca-O separations emerge (i.e. the left, middle and right peaks) as the Ca moves off-centre within the dodecahedral site. The Ba-O separation shows the potential formation of shoulders on the main peak suggesting distortions within the regular dodecahedra and also the appearance of a small peak at larger Ba-O separations. This is caused by the shorter Ca-O separations that out-compete the Ba-O interaction and pull the O further from the Ba. In BST the Sr and Ba both show similar behaviour to the Ba in BCT with one main broad peak and a small peak at larger separations of A-O which is caused by the local arrangement of the Sr and Ba where the Sr will potentially out-compete the Ba in some cases and in others the Sr will fail to fully fill the dodecahedra and some Oxygen anions will be pulled in by the Ti. Overall the analysis suggests only the

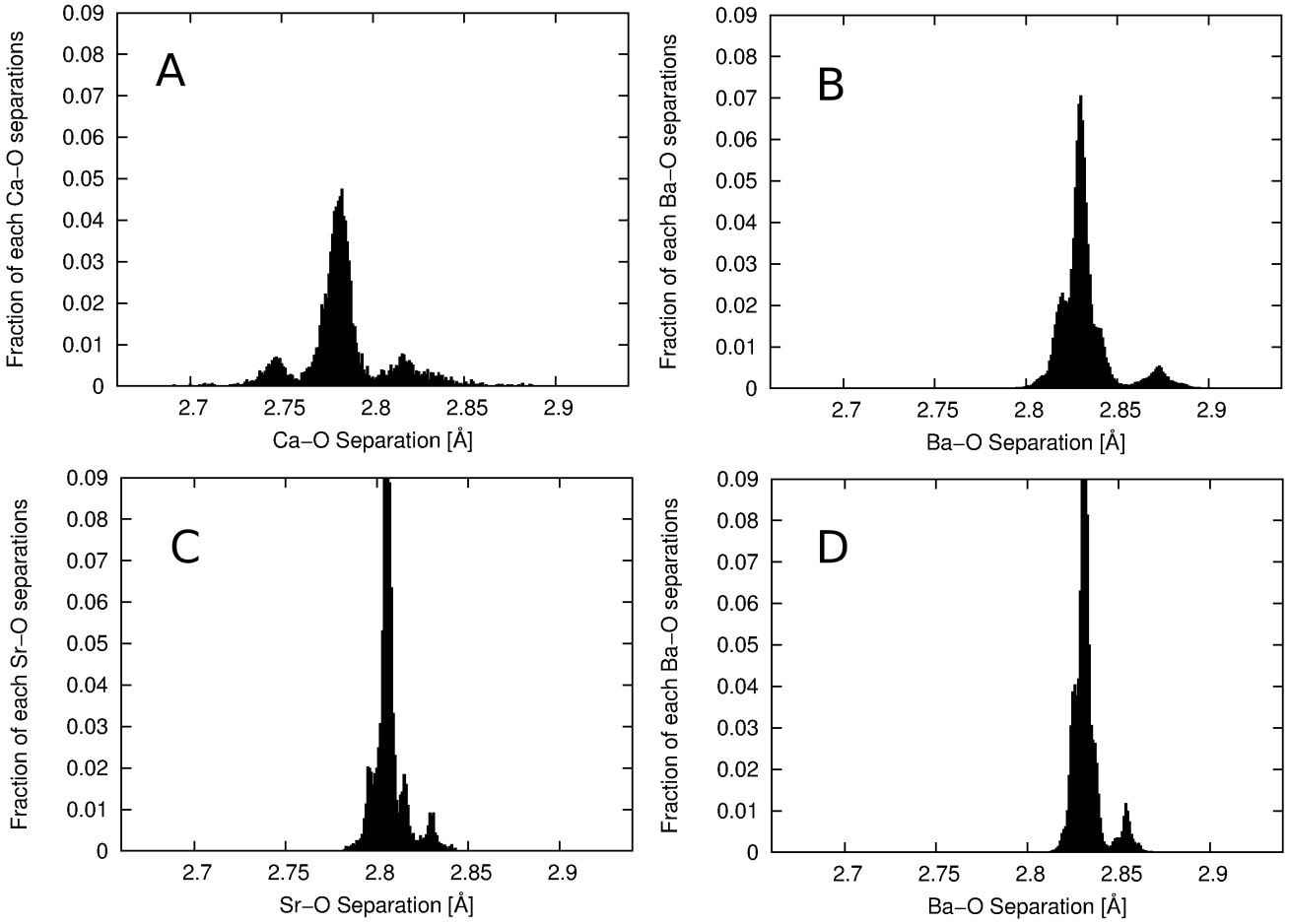

Figure 5: Distribution of A-O separations. (A) Ca-O in BCT; (B) Ba-O in BCT; (C) Sr-O in BST; (D) Ba-O in BST for x=0.08. Ba-O = 2.833 Å in BT, Ca-O =2.3-2.72 Å in CT and Sr-O = 2.802 Å in ST for reference.

Ca, and not the Sr, is undergoing a significant relaxation and change in coordination.

The two potential relaxations that have been suggested for the Ca cation in the literature are in the [111] and [001] directions which lead to two different coordination values as shown in Figure 6. The [111] relaxation will move the cation towards the corner of the dodecahedra creating 3 short Ca-O, 6 medium Ca-O and 3 long Ca-O ($\sim$9 coordinate - termed 3+6+3), while the [001] relaxation moves the Ca closer to one side of the dodecahedra generating 4 short Ca-O, 4 medium Ca-O and 4 long Ca-O ($\sim$8 coordinate - termed 4+4+4). This is shown schematically in Figure 6.

To identify the relaxation taking place around the Ca it is necessary to determine if the peaks observed correspond to a 4+4+4 coordinate system or a 3+6+3 coordinate system. This can be done by examining the difference between different Ca-O separations. Figure 5 shows the width of the main (middle) peak is approximately 0.04 Å for Ca-O separations. As this main peak covers the whole unrelaxed dodecahedra it implies the total variation of the Ca-O separations in a regular 12 coordinate dodecahedra should be $<$0.04 Å. Similarly the separation between the smallest and largest peaks which correspond to the short and long Ca-O separations formed by the Ca relaxation is $\sim$0.05 Å. Therefore, by identifying all the Ca sites which have a difference between the longest and shortest Ca-O separations of $>$0.05 Å we can identify all those Ca sites undergoing a significant relaxation. This is shown in Table 4 and can be seen to increase with Ca content. Note that even near the solid solution limit not all the Ca sites are undergoing a relaxation away from 12-coordination. In a similar manner to that observed for the octahedral volume we see a mix of different local structures emerging within the solid solution and one uniform model does not describe all of the sites. The advantage of using classical simulations is the ability to model multiple cells of large size. This demonstrates the solid solution of BCT is far from homogeneous with lots of local variation and therefore multiple local Ca environments. This would be extremely difficult to model with DFT or experimental techniques that generate system averages.

To identify the type of relaxation it is necessary to compare the difference in size of the Ca-O separations as indicated in Figure 7. In the 3+6+3 relaxation the 3rd shortest Ca-O separation should be significantly smaller than the 3rd longest Ca-O separation as each belongs to different grouping of Ca-O separations i.e. short vs long. The 4th shortest Ca-O separation will, however, be a similar size to the 4th longest Ca-O separation as both these separations will be in the medium Ca-O separation group. In the case of the 4+4+4 relaxation, both the 3rd and 4th shortest are both within the short Ca-O group and the 3rd and 4th longest are both in the long Ca-O group. There will, therefore, be a significant difference in the size of both the 3rd shortest and 3rd longest and 4th shortest and 4th longest if the 4+4+4 relaxation is taking place. The 5th shortest and 5th longest Ca-O separations will, however, be in the same medium Ca-O group and therefore should be approximately the same size.

Table 4: Percentage of Ca undergoing relaxation towards 4+4+4 coordination at a given mole fraction.

Mole fraction	Percentage
0.0058	0 %
0.035	14.0 %
0.079	26.1 %
0.117	36.3 %
0.146	41.1 %
0.20	47.9 %
0.239	52.1 %

In Figure 8 the difference in size between the Ca-O separations is plotted along the x-axis and the frequency of Ca sites with this difference is plotted along the y axis. The difference between the 3rd shortest Ca-O and 3rd longest is plotted in Figure 8A, the difference between the 4th shortest and 4th longest is plotted in Figure 8B, and the difference between the 5th shortest and 5th longest is plotted in Figure 8. The implications of this are that most of the relaxed Ca-O sites are adopting a 4+4+4 relaxation as we observe a similar frequency of large differences between the 4th shortest and 4th longest and the 3rd shortest and 3rd longest. This suggests that the majority of Ca relaxations are in the [001] direction.

In summary as the mole fraction of Sr increases

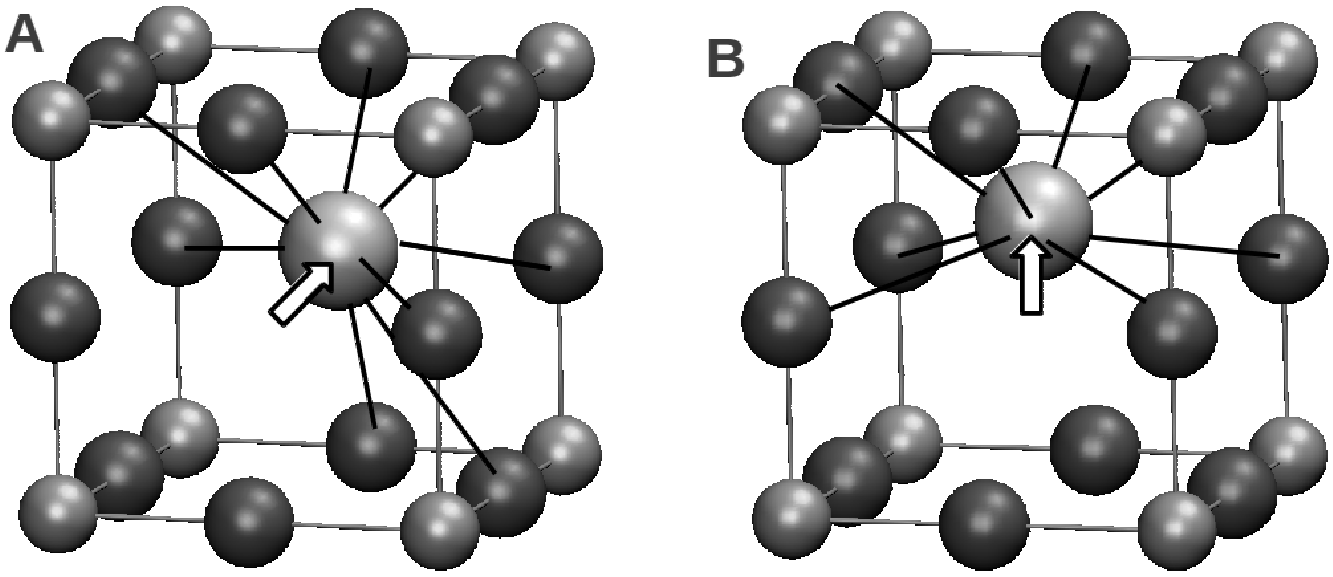

Figure 6: A representation of the Ca cation relaxation in the (A) [111] direction and (B) the [001] direction. The new coordination shell of nearest Oxygens anions are highlighted with bonds. The [111] direction generates a 9 coordinate shell and the [001] direction generates a 8 coordinate shell.

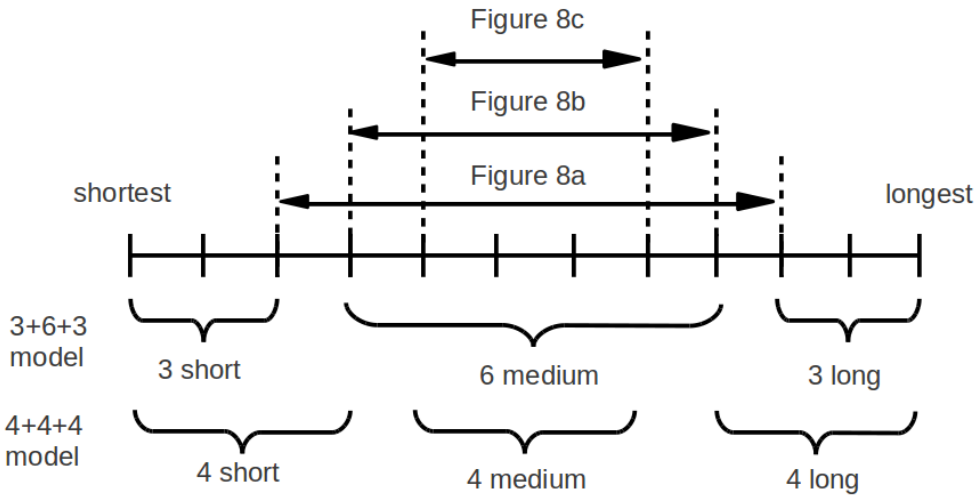

Figure 7: Schematic diagram showing the different Ca-O separations depending on the relaxation direction. The central blue bar indicates the Ca-O separation with the 12 different Ca-O separations listed left to right shortest to longest. The curly brackets indicate the groupings of the Ca-O separations (i.e. the number in each group that will have the same size Ca-O separation) that will result from the two different relaxations e.g. the 3+6+3 result produces 3 short Ca-O separations that are all have approximately the same size, 6 medium that are approximately the same size and 3 long that are approximately the same size. Also shown are the distances calculated for Figure 8 with the black arrows. These are the difference in size between different Ca-O separations. Differences greater than 0 will exist when the two Ca-O separations being compared belong to different groupings.

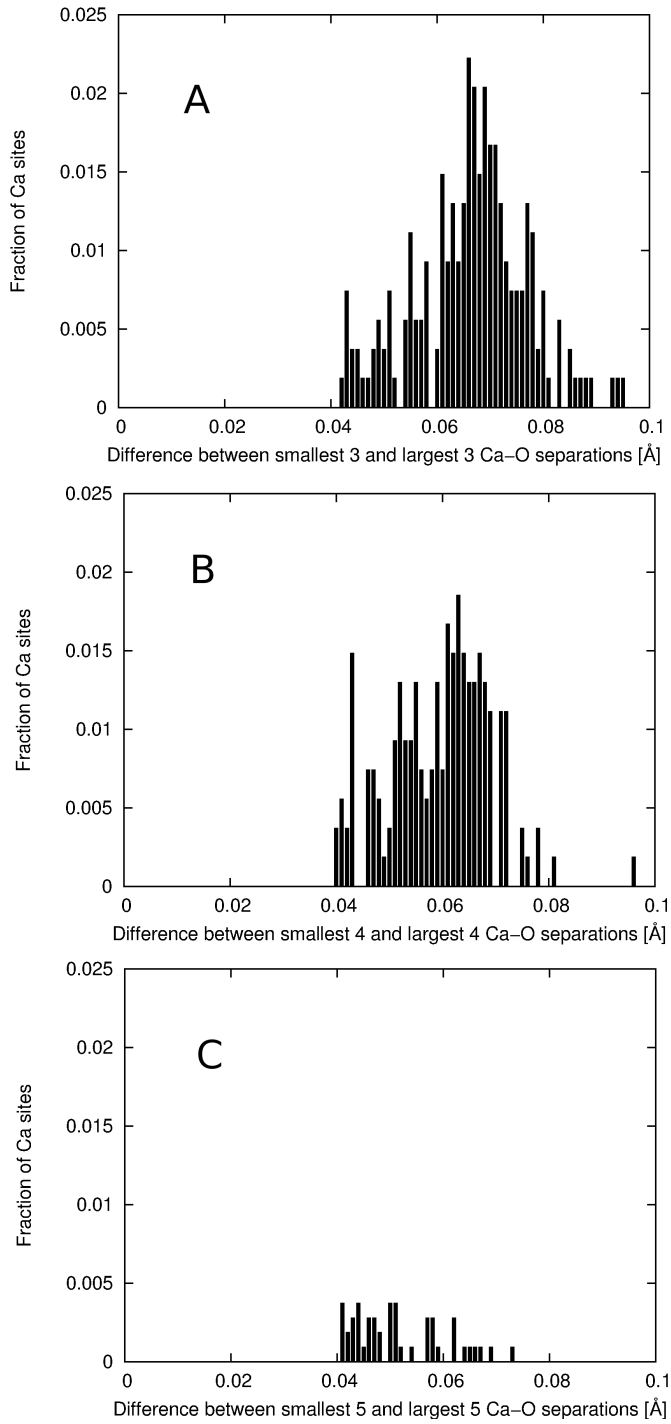

Figure 8: Fraction of Ca sites with particular differences between the shortest and longest Ca-O separations. (A) 3 smallest and 3 largest; (B) 4 smallest and 4 largest; (C) 5 smallest and 5 largest for x=0.12

in BST the whole cell shrinks. The TiO_6 octahedra reduce in volume and the A-O separations shrink. Although some disorder within the polyhedra occurs the structure remains relatively regular. In BCT there is a shrinkage of the TiO_6 octahedra with increasing Ca content but these octahedra also become very irregular with some remaining the same size as in undoped BT and many demonstrating large local relaxations. Additionally, some of the Ca cations displace in the [001] direction generating a more 8 coordinate system as observed in $CaTiO_3$.

BST Enthalpy and Volume of Mixing

Earlier we highlighted the larger than expected negative ΔH_{mix} and ΔV_{mix} at low concentrations of Ba in ST. Examination of these structures indicates this is largely a feature of formation of some particular small unit cells that form. When a single Ba is surrounded by Sr sites only the Ba-O interaction is out-competed by the Sr-O interaction (due to the smaller size of the Sr) and some of the Sr-O separations shrink significantly and the Sr moves slightly off-centre within the dodecahedra. This is a low energy configuration as the Sr-O interactions are able to shrink significantly (closer to their values in the ideal SrO oxide) generating very low energy interactions. The configuration also has a smaller volume due to the off-centring of the Sr which causes the cell to shrink further than expected. Although most of the configurations are more regular with the solid solution mix these configurations are low in energy and therefore contribute significantly to the overall thermodynamics of the solid solution. We can observe their formation by examining the spread of the Sr-O and Ba-O separations as indicated by their standard deviation (Table 5).

Table 5: Mean average Sr,Ba-O separations in $Sr_xBa_{(1-x)}TiO_3$. The standard deviations are listed after the $\pm$.

Mole fraction of Sr	Sr-O	Ba-O
0.9375	2.802 ± 0.017	2.830 ± 0.014
0.875	2.802 ± 0.032	2.830 ± 0.021
0.8125	2.802 ± 0.022	2.831 ± 0.017
0.75	2.802 ± 0.013	2.830 ± 0.014

Implications for T_c

The reduction in the TiO_6 octahedral volume will impede the formation of the tetragonal ferroelec-

tric phase since the Ti have less space available in which to move off centre. The shrinking size of the octahedra in BST will, therefore, reduce T_c as the ferroelectric phase becomes less stable and harder to form.

The behaviour of T_c in BCT is more complicated with a small increase until x=0.08 and then a decline beyond this. There are two factors involved in this process. Firstly, the general size of the octahedra is reducing which will impede the ferroelectric relaxation. Disorder, however, in the octahedra is also very prevalent. This disorder will potentially allow the octahedra to adopt a dipole despite the small size as the structure distorts. Coupled with this is the wide range of volumes reported within the solid solution mixes; even at large values of x some of the octahedra still have a volume comparable to BT and it can be assumed that these octahedra would still also be capable of a ferroelectric relaxation. We would, therefore, expect the effect of volume contraction to be smaller in the case of BCT compared to BST and the decline should be more gradual - such a result has also been suggested by Levin *et al.*[12] The second factor is the Ca cations. The Ca cations are capable of contributing to the ferroelectric effect by going off-centre within the dodecahedra. The Ca cation is too small for the site and we observe many Ca going off centre creating a 4+4+4 coordination which will generate a dipole. As this relaxation is in the direction of the lattice axis (i.e. [001]) it will also be in the same direction as that of the Ti and therefore the two effects can combine. Table 4 lists the percentage of Ca cations undergoing the relaxation in the solid solution range. This increases with x but the rate of increase declines with increasing x. So, overall, there is a positive contribution to T_c from the off-centring of the Ca cations throughout the solid solution phase competing against the shrinking of the TiO_6 octahedra.

We can attempt to apply a simple empirical relationship to the values identified as controlling T_c within BCT and BST. An approximately linear relationship exists between the mole fraction of Sr in BST and the value of T_c from experiment[26] and a similar approximately linear relationship between the mole fraction of Sr in BST and the mean TiO_6 octahedral volume is observed here. This implies we can fit a simple straight line equation for the octahedral volume and T_c by using experimental values of T_c for BT and ST[27] as two points of our line,

$$T_c = mV - c, \tag{2}$$

where m is 847.1 KÅ^{-3}, c is 8676.1 K and V is the mean octahedral volume in Å^{-3}. For BCT we must also account for the effects of the Ca. The results in Table 4 suggest we can fit the relationship between the number of ferroelectrically relaxed Ca and the mole fraction using a simple exponential relationship of,

$$F = A[1 - \exp(-Dx)], \tag{3}$$

where F is the fraction of CaO_{12} sites undergoing the ferroelectric relaxation, A is the maximum fraction undergoing relaxation, D is a prefactor and x is the mole fraction of Ca. Performing a regression analysis, A is fitted as 0.60, and D as 7.83 with a square of the residual fit R^2 = 0.0012. Assuming that each Ca site undergoing a ferroelectric relaxation will contribute half the ferroelectric response as a Ti site if both ions undergo a similar sized relaxation and given the nominal charges of Ca^{2+} versus Ti^{4+} i.e. for a potential total T_c of 201.5 K with all Ca relaxed (half of the standard value for BT of 403 K). Experimental analysis suggests a total contribution of $\sim \frac{1}{3}$ that of Ti site[12] but simulations, in contrast, have suggested a relaxation larger than the Ti site[14] so the assumption of half appears reasonable value lying between these estimates. Assuming we can simply combine the effects of Ca relaxation and octahedral volume changes, we obtain a relationship of

$$T_c = 847.1V - 8676.1 + 201.5F. \tag{4}$$

This relationship is plotted for both BST and BCT along with experimental values in Figure 9. This empirical relationship closely describes the variation of T_c in BCT with a peak at x=0.08 of 413 K and then a gradual decline. Clearly the behaviour of T_c is more complicated than this model alone which will explain the differences between experiment and theory. For example, we do not account for the disorder of the octahedra which will probably reduce the rate of decline of T_c particu-

larly in BCT. The empirical relationship is, however, a useful potential guide to the ferroelectric behaviour of the system and suggests the local atomic behaviour we report can be used to understand the experimental results observed for T_c variation in BST and BCT.

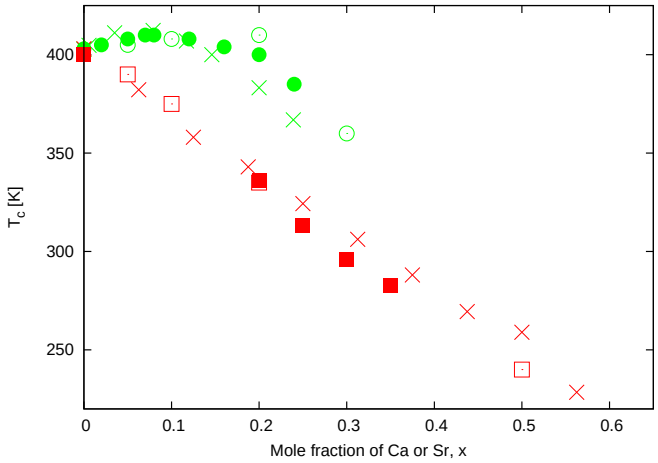

Figure 9: Prediction of T_c with varying mole fraction x for $Ba_{1-x}Sr_xTiO_3$ (red crosses) and $Ba_{1-x}Ca_xTiO_3$ (green crosses) and comparison with experiments for $Ba_{1-x}Sr_xTiO_3$ (red squares) and $Ba_{1-x}Ca_xTiO_3$ (green circles). BCT data taken from (filled circles)[6] and (open circles),[12] BST data taken from (filled squares)[28] and (open squares).[24]

Supporting Information Available: Supplementary information showing the A-O separations for other solid solution mixes is available online. This material is available free of charge via the Internet at `http://pubs.acs.org`.

References

(1) Anwar, S.; Sagdeo, P. R.; Lalla, N. P. *Journal Of Physics-Condensed Matter* **2006**, *18*, 3455–3468.

(2) Hennings, D.; Schnell, A.; Simon, G. *Journal Of The American Ceramic Society* **1982**, *65*, 539–544.

(3) Hotta, Y.; Hassink, G.; Kawai, T.; Tabata, H. *Japanese Journal Of Applied Physics Part 1-Regular Papers Short Notes & Review Papers* **2003**, *42*, 5908–5912, 20Th Meeting On Ferroelectric Materials And Their Applications (Fma 20), Kyoto, Japan, May 28-31, 2003.

(4) Zheng, R.; Wang, J.; Tang, X.; Wang, Y.; Chan, H.; Choy, C.; Li, X. *Journal Of Applied Physics* **2005**, *98*, 084108.

(5) Zhang, L.; Thakur, O. P.; Feteira, A.; Keith, G. M.; Mould, A. G.; Sinclair, D. C.; West, A. R. *Applied Physics Letters* **2007**, *90*, 142914.

(6) Mitsui, T.; Westphal, W. *Physical Review* **1961**, *124*, 1354–1359.

(7) Freeman, C. L.; Harding, J. H.; Cooke, D. C.; Elliot, J. A.; Lardge, J. S.; Duffy, D. M. *Journal Of Physical Chemistry C* **2007**, *111*, 11943–11951.

(8) Tang, X.; Chew, K.; Wang, J.; Chan, H. *Applied Physics Letters* **2004**, *85*, 991–993.

(9) Saha, S.; Sinha, T.; Mookerjee, A. *European Physical Journal B* **2000**, *18*, 207–214.

(10) Mather, G. C.; Islam, M. S.; Figueiredo, F. M. *Advanced Functional Materials* **2007**, *17*, 905–912.

(11) Sinclair, D. C.; Attfield, J. P. *Chemical Communications* **1999**, *16*, 1497–1498.

(12) Levin, I.; Krayzman, V.; Woicik, J. C. *Applied Physics Letters* **2013**, *102*, 162906.

(13) Krayzman, V.; Levin, I.; Woicik, J. C.; Bridges, F.; Nelson, E. J.; Sinclair, D. C. *Journal Of Applied Physics* **2013**, *113*, 044106.

(14) Okajima, T.; Yasukawa, K.; Umesaki, N. *Journal Of Electron Spectroscopy And Related Phenomena* **2010**, *180*, 53–57.

(15) Fu, D.; Itoh, M.; Koshihara, S.-Y.; Kosugi, T.; Tsuneyuki, S. *Physical Review Letters* **2008**, *100*, 227601.

(16) Gale, J. D.; Rohl, A. L. *Molecular Simulation* **2003**, *29*, 291–341.

(17) Dick, B. G.; Overhauser, A. W. *Physical Review B* **1958**, *112*, 90.

(18) Harding, J. *Reports On Progress In Physics* **1990**, *53*, 1403–1466.

(19) Freeman, C. L.; Dawson, J. A.; Chen, H.-R.; Harding, J. H.; Ben, L.-B.; Sinclair, D. C. *Journal Of Materials Chemistry* **2011**, *21*, 4861–4868.

(20) Dawson, J. A.; Li, X.; Freeman, C. L.; Harding, J. H.; Sinclair, D. C. *Journal Of Materials Chemistry C* **2013**, *1*, 1574–1582.

(21) Freeman, C. L.; Dawson, J. A.; Chen, H.-R.; Ben, L.; Harding, J. H.; Morrison, F. D.; Sinclair, D. C.; West, A. R. *Advanced Functional Materials* **2013**, *23*, 3925–3928.

(22) Matra, D. *Ferroelectric Ceramics*; Maclaren And Sons Ltd: London, 1966.

(23) Lee, S.; Levi, R. D.; Qu, W.; Lee, S. C.; Randall, C. A. *Journal Of Applied Physics* **2010**, *107*, 023523.

(24) Levin, I.; Krayzman, V.; Woicik, J. C. *Physical Review B* **2014**, *89*, 024106.

(25) Park, J.-S.; Lee, Y.-H.; Kim, K.-B.; Kim, Y.-I. *Nuclear Instruments & Methods In Physics Research Section B-Beam Interactions With Materials And Atoms* **2012**, *284*, 44–48.

(26) Vendik, O.; Zubko, S. *Journal Of Applied Physics* **2000**, *88*, 5343–5350.

(27) Trainer, M. *European Journal of Physics* **2000**, *12475-4*, 459–464.

(28) Ianculescu, A.; Berger, D.; Mitoseriu, L.; Curecheriu, L. P.; Drgan, N.; Crisan, D.; Vasile, E. *Ferroelectrics* **2008**, *369*, 22–34, 11Th European Meeting On Ferroelectricity (Emf-2007), Bled, Slovenia, Sep 03-07, 2007.

Supplementary Information

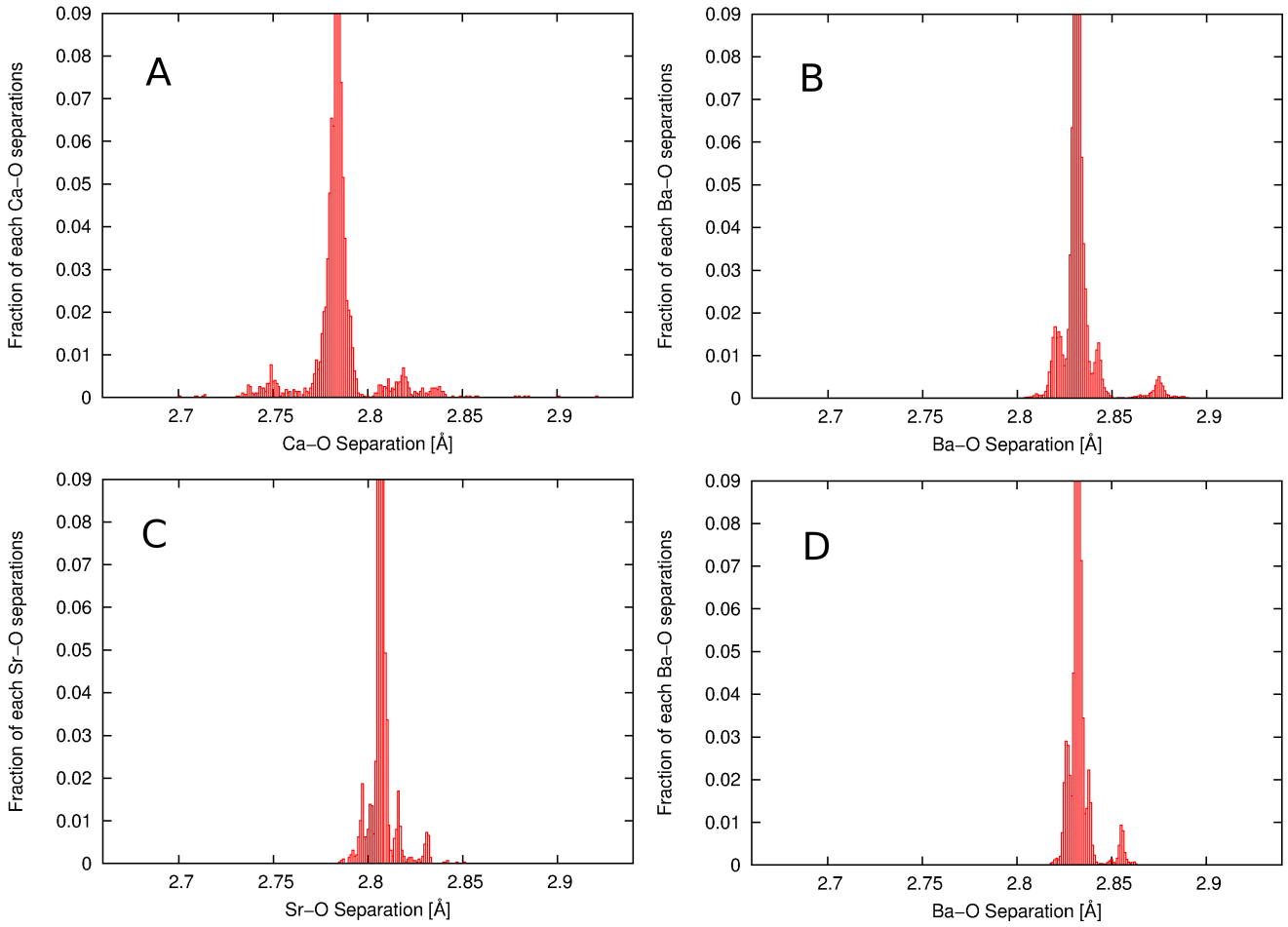

Figure S10: Distribution of A-O separations. (A) Ca-O in BCT; (B) Ba-O in BCT; (C) Sr-O in BST (D) Ba-O in BST for x=0.035

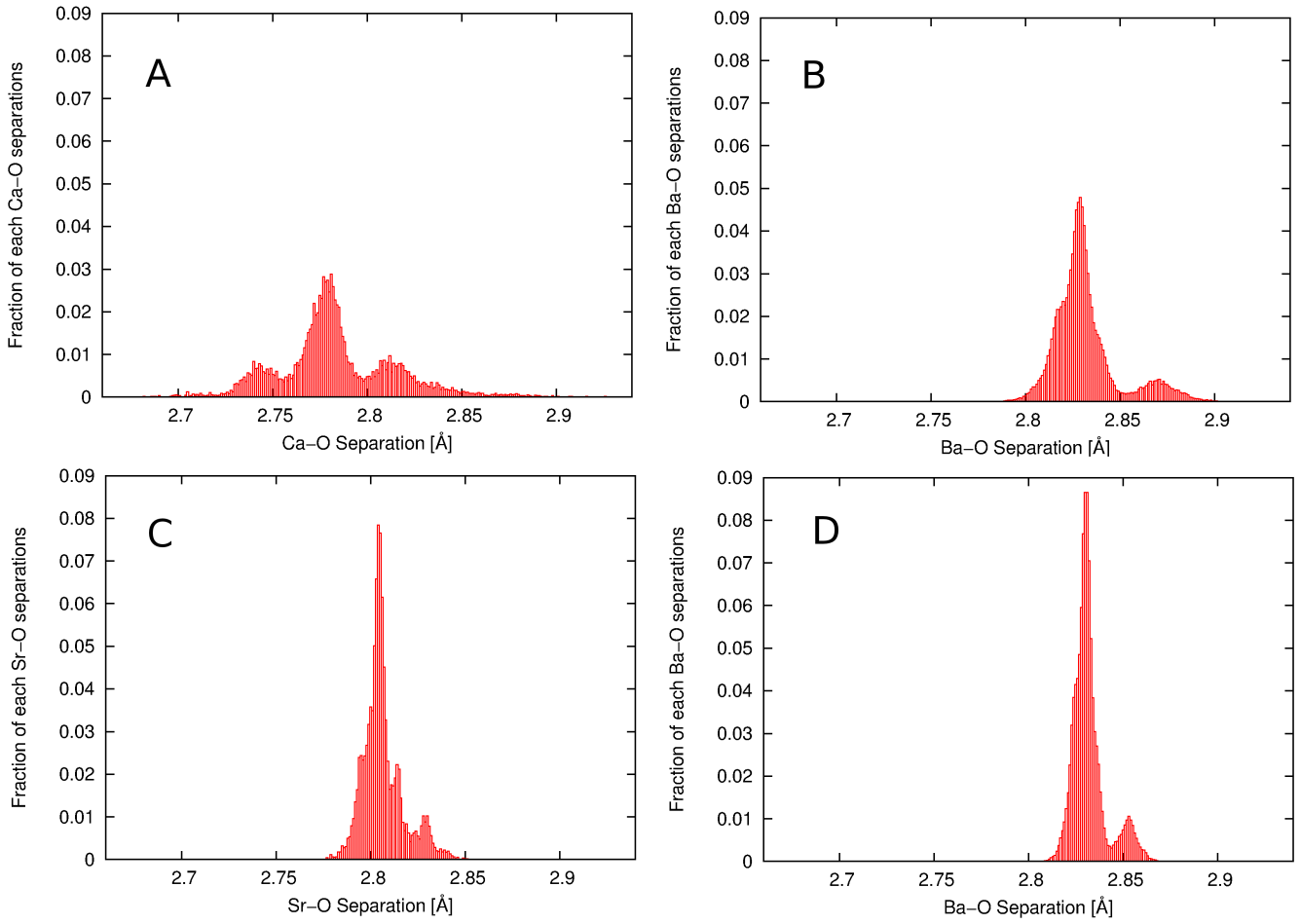

Figure S11: Distribution of A-O separations. (A) Ca-O in BCT; (B) Ba-O in BCT; (C) Sr-O in BST; (D) Ba-O in BST for x=0.12

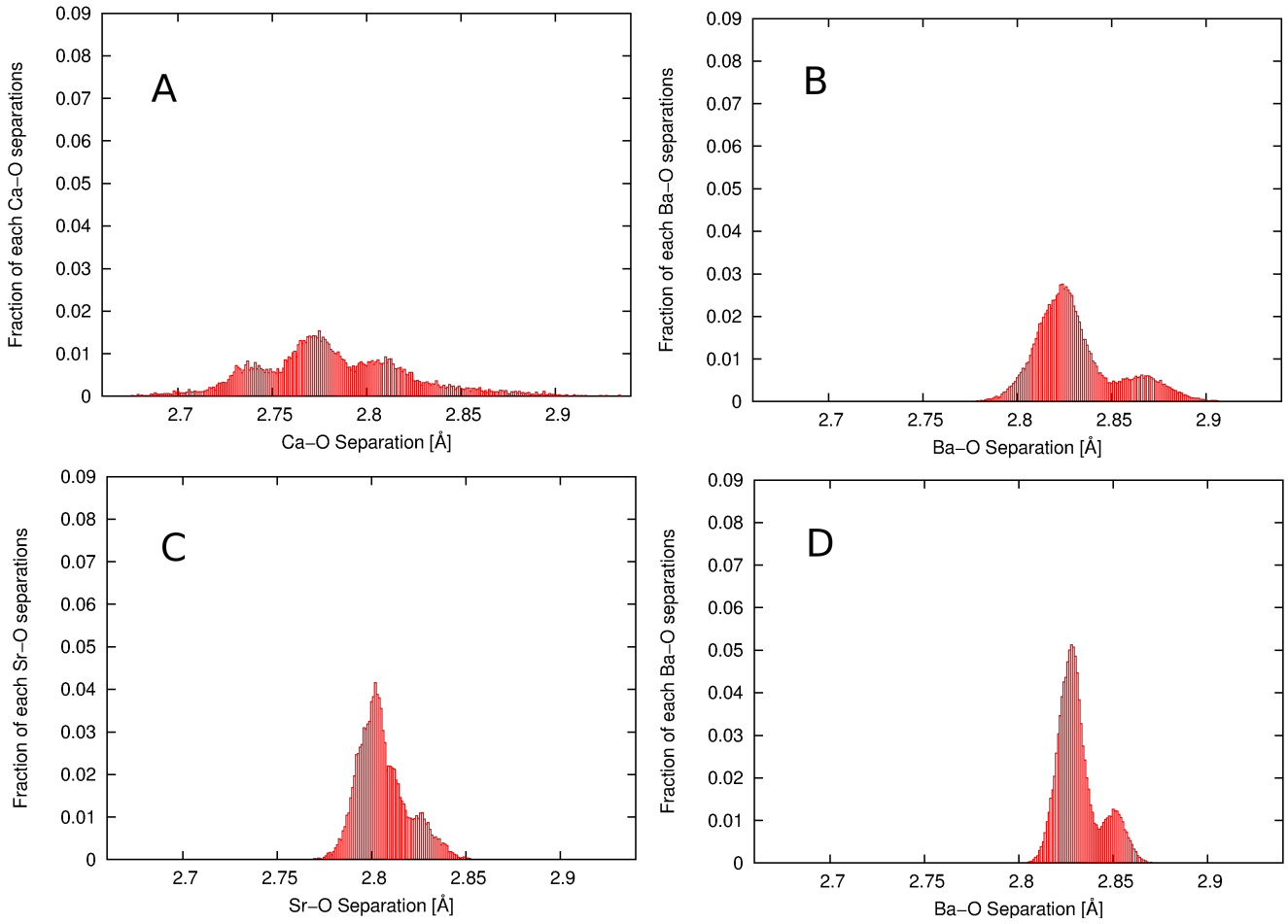

Figure S12: Distribution of A-O separations. (A) Ca-O in BCT; (B) Ba-O in BCT; (C) Sr-O in BST; (D) Ba-O in BST for x=0.198

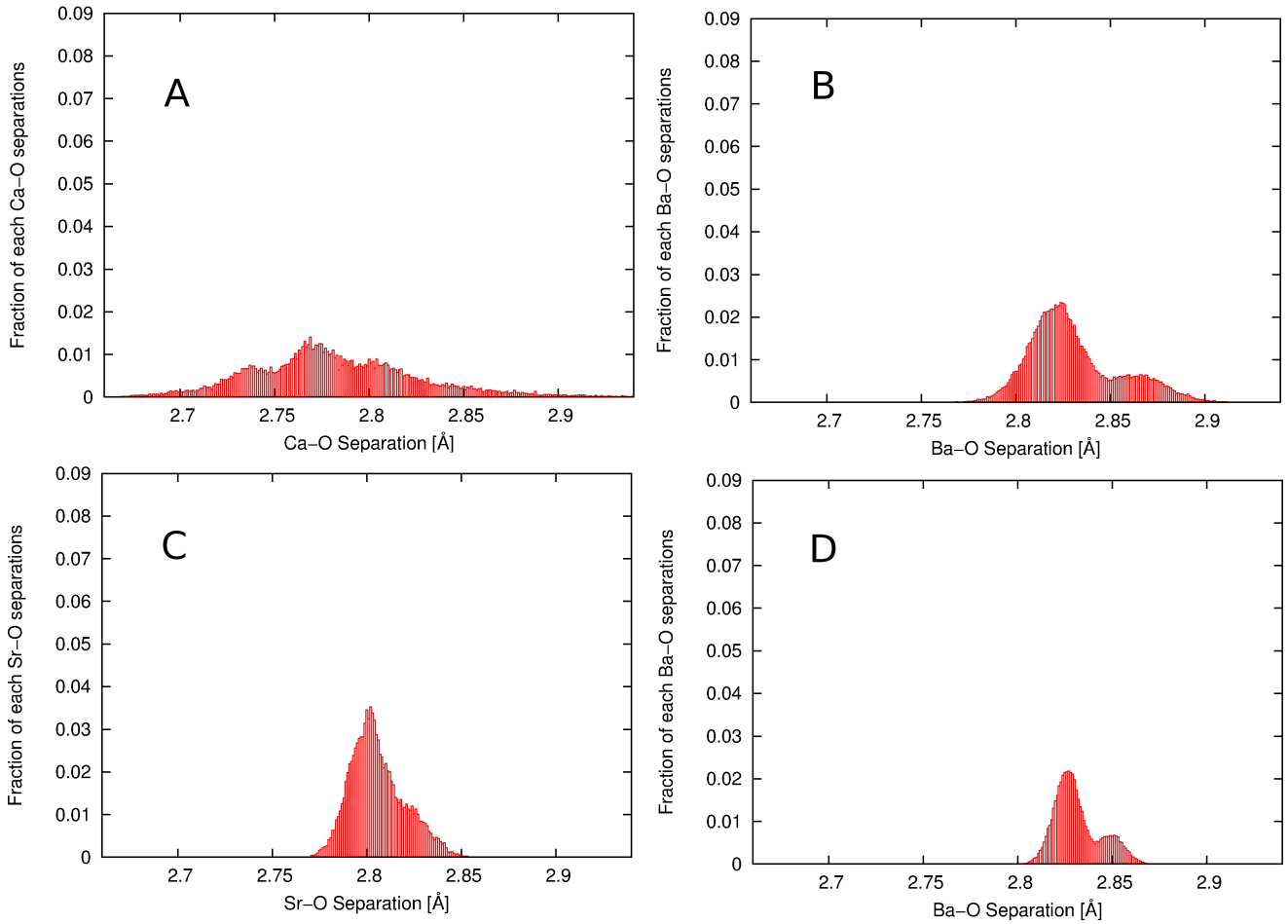

Figure S13: Distribution of A-O separations. (A) Ca-O in BCT; (B) Ba-O in BCT; (C) Sr-O in BST; (D) Ba-O in BST for x=0.239

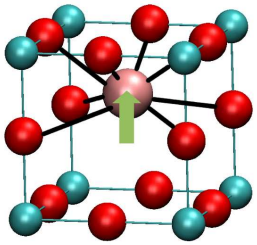

Figure S14: Table of Contents Image.